Application of dynamic optical tomography for the detection of a multi-phase physiologic response to Valsalva maneuver in healthy and diseased breast tissue

R. E. Hardin[1], D. P. Klemer[1,2], M. S. Katz[1], N. A. Franco[1], H. L. Graber[1,2], C. H. Schmitz[1,2], R. L. Barbour[1,2], A. G. Smeraldi[3] and T. F. Panetta[3]

[1]SUNY Downstate Medical Center, [2]NIRx Medical Technologies, LLC and [3]SUNY Downstate Medical Center, and Staten Island University Hospital

INTRODUCTION

DYnamic **N**ear-Infrared **O**ptical Tomography (DYNOT) is presently being applied to investigations of brain imaging, peripheral vascular imaging and studies of benign and malignant breast lesions. This relatively new technology differs from modalities currently in use in that DYNOT is a quantitative analysis of vascular bed reactivity and function. Needed in this analysis is a provocation that produces a coherent response in the area of study that is both repeatable and has the ability to differentiate healthy from diseased tissue. This provocation must disturb the normal microcirculation in the tissue volume under study resulting in changes in blood volume, providing the necessary dynamic changes for optical imaging using DYNOT technology. Since imaging is done on a dynamic scale, this allows for detection of spatiotemporal changes in blood volume and hemoglobin states within tissue, permitting identification of dysfunctional tissue exhibiting altered vascular reactivity. One externally-imposed provocation investigated here is the Valsalva maneuver. The elicited hemodynamic changes and the spatiotemporal response to these provocations can be measured and imaged tomographically. A Valsalva maneuver, described as forced expiration against a closed glottis, consists of four distinct phases, corresponding to specific physiologic changes (Figure 1).

Valsalva Maneuver

Definition of Valsalva Maneuver: Forced, maximal expiration, generating a pressure of 40 mmHg for at least 10 seconds, against a closed glottis, serving to increase both intra-thoracic and intra-abdominal pressure, resulting in changes in arterial blood pressure.

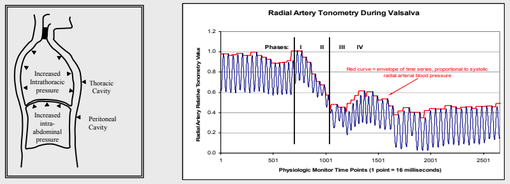

Fig 1. Schematic diagram showing increased intra-abdominal and intrathoracic pressures (left) developed during the Valsalva maneuver, along with a typical blood pressure tracing (right) recorded from a right radial artery tonometer. (The tracing has been low-pass filtered to reduce high-frequency noise.)

As is evident from the radial artery tonometry tracing in Figure 1, the straining evoked by the Valsalva maneuver at the initiation of Phase 1 causes an abrupt increase in both intrathoracic and intraabdominal pressure. This change compresses the central vasculature and causes increased blood delivery to the periphery. This subsequently leads to changes in arterial blood pressure. Phase 1 occurs almost immediately after the onset of the Valsalva maneuver and is marked by an increase in arterial blood pressure and slowing of the heart rate due to baroreceptor activation. The arterial blood pressure will then fall, concomitant with an increase in heart rate which marks Phase 2 of the response, again due to baroreceptor response to a fall in cardiac output from compromised venous return to the heart. Phase 3 occurs with the release of straining which leads to a further drop in blood pressure and acceleration of the heart rate, which is transient compensation for sudden loss of compression of the aorta. In the final phase of this physiologic response, the blood pressure overshoots the baseline value before returning to normal, and the heart rate decreases [2]. The current capability of DYNOT imaging allows one to not only detect this physiologic behavior but to also differentiate the four phases of the physiologic response in real time. This is of clinical importance, as this finding can be utilized to evaluate differential responses in tissues transformed by neoplastic processes compared to normal tissue.

We will present results from subjects with and without breast disease and will construct mathematical models of the measured response to this maneuver. Parameters of our mathematical modeling can then be used to compare data obtained from diseased tissue to identify areas of abnormal response, indicating the presence of abnormal vascular reactivity. As we will demonstrate, the valsalva maneuver is a repeatable provocation that effects the entire breast and is able to differentiate healthy tissue from diseased.

THE INSTRUMENTATION

A multi-channel continuous wave near-infrared optical tomographic imager (DYNOT System, NIRx Medical Technologies, LLC., Glen Head, NY 11545), operating at 760 nm and 830 nm, was used for all measurements. In Figure 1 we show a functional layout of the imager with expanded views of the instrument set-up and real-time data display screens. Depicted is a four-level functionality scheme comprising system hardware, system control, data analysis and image display. The basic system provides for frequency encoding having a capability of up to four laser diode sources, a fast optical switch with incoupling optics, use of various measuring heads, a multichannel parallel detector module equipped with adjustable gain control, and a system controller.

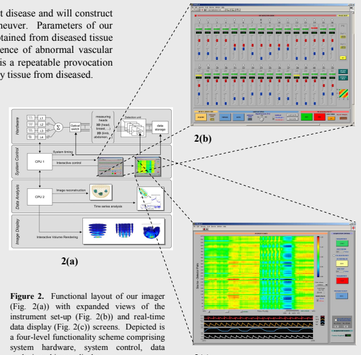

Figure 2. Functional layout of our imager (Fig. 2(a)) with expanded views of the instrument set-up (Fig. 2(b)) and real-time data display (Fig. 2(c)) screens. Depicted is a four-level functionality scheme comprising system hardware, system control, data analysis and image display.

THE INSTRUMENTATION (cont'd)

Dynamic measurements were performed using a measurement head which directs near-infrared light onto the subject's breast via multiple arrays of optical fibers mounted in a secure frame. Each optode delivers approximately 20 mW of optical power for a period of 10 ms per cycle, producing a flux of ~10 mJ·s^{-1}·cm^{-2}. Dual-wavelength optical energy at wavelengths 760nm and 830nm was used for imaging in a time-multiplexed fashion, such that a complete scan of the breast is accomplished in approximately 400 milliseconds. Measuring heads are available for both single-breast and simultaneous dual-breast measurements. Figure 3 shows a close-up view of the dual-breast measuring head, with white silicone phantoms in place, used for system testing.

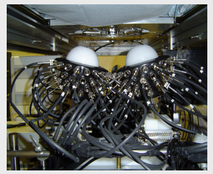

Figure 3. Photograph of measuring head used for simultaneous dual-breast measurements. Thirty-one source-detector fibers are distributed over the surface of each breast.

METHODS

Six female subjects were enrolled in this study; two subjects had unilateral breast cancer, two subjects had unilateral non-neoplastic breast disease (one galactorrhea and one breast cyst) and two subjects were healthy volunteers. Data collection was performed using an adjustable hemispherical DYNOT breast measuring head supporting 25 source fibers and 29 detector fibers for a unilateral breast scan. Each breast was imaged separately. Each subject was placed prone in the breast imager with the breast held pendant within the measuring head. Baseline measurements were then obtained for 1000 time points (approx. 7 minutes). The subject then performed the Valsalva maneuver, maintaining a pressure of 40 mmHg against a fixed resistance. The subject was allowed to recover to baseline for at least 500 time points. This was performed three times.

DATA ANALYSIS and RESULTS

Figure 4 shows the resulting spatially-averaged normalized oxyhemoglobin time series of the left and right breast, performed on a healthy volunteer**.** Evident in the tracing is a drop in oxyhemoglobin as the subject inspires just prior to the initiation of Phase 1 of the Valsalva, resulting from a blood volume decrease due to increased negative intrathoracic pressures secondary to inspiration. Figure 5 presents a magnified view of a single Valsalva, with the four dynamic Valsalva phases identified.

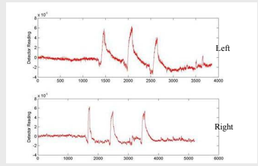

Figure 4. Spatially-averaged oxyhemoglobin time series recorded from the left and right breasts of a healthy volunteer during a sequence of three Valsalva maneuvers, each separated by a 200-second resting interval

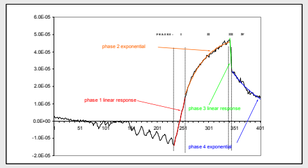

Figure 5. Approach to mathematical modeling of a classic Valsalva response manifested in the spatially-averaged oxyhemoglobin time series, showing linear approximation of the first and third phases, and an exponential model of the second and fourth phases.

Derivation of a metric which can potentially be used to compare healthy and diseased tissue begins with a mathematical modeling of the four individual phases, as shown in Figure 5. The rapid changes associated with onset of straining and release of Valsalva pressure (phases 1 and 3) are most accurately modeled with a linear slope. In cases where a subject can sustain the Valsalva for a sufficiently-long duration, the Phase 2 time behavior becomes apparent, and can best be modeled as an exponential solution to a first-order linear differential equation. Similarly, the Phase 4 "return to baseline" dynamic behavior is also modeled as an exponential function.

We analyzed the Valsalva responses of 12 breasts from 6 patients, each of which showed the classic Valsalva behavior typified by the mean time series shown in Figure 4. Using the mean times series as a model function, each time series was analyzed for percentage of variance accounted for by model function. This analysis was performed for oxygenated (Oxy-Hb), reduced (Red-Hb), and total (Tot-Hb) hemoglobin. We then proceeded to perform derivative analysis of all phases of the Valsalva curve, using a standard Matlab multidimensional unconstrained nonlinear function minimization. We found that we could consistently and reliably model the first, third and fourth phases therefore, these three phases were chosen for subsequent data analysis.

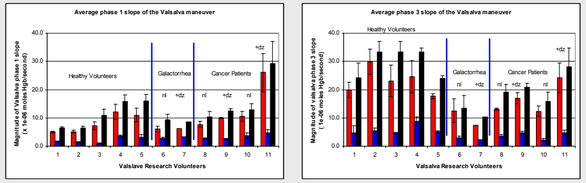

Figure 6. Mean Valsalva Phase 1 and Phase 3 rates-of-change for 11 experiments (error bars represent one standard deviation).

Figure 6 demonstrates the mean value of the modeled rates-of-change for the first and third phases of the Valsalva maneuver in 11 of our 12 measurements. It is clearly evident that Phase 3 rates tend to be higher than Phase 1 rates. This trend holds true for oxyhemoglobin, deoxyhemoglobin and total hemoglobin. This suggests that vascular filling of the breast tissue during phase 1 tends to be a slower process than vascular drainage during the release of straining, on a gross, spatially-averaged level.

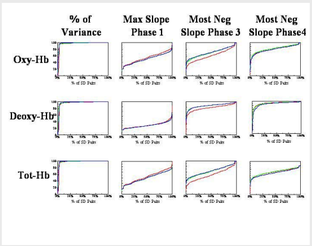

Figure 7. Rank ordered plots of values for source-detector pairs (SD pairs) for Oxy-Hb, Deoxy-Hb and Tot-Hb. The Percentage of Variance shows that the provocation effects the entire breast. The three slope analyses show that the effect of the provocation is repeatable.

Each performed Valsalva was analyzed separately. The results for percentage of variance and derivative analysis for oxygenated, reduced and total hemoglobin were then rank ordered and plotted. The first column of Figure 7 under "% of Variance" shows that for the percentage of variance accounted for by the model function is equal to or greater than 95% in 94% of source detector pairs (SD pairs) for Oxy-Hb and Tot-Hb and in 92% of SD pairs for Deoxy-Hb

The next step in our investigation of the Valsalva maneuver for use as a provocation was to examine dynamic behavior on a pixel level, after tomographic image reconstruction. We have implemented an analysis approach in which the near-infrared data is used to create three-dimensional pixel maps. Figure 8 illustrates such a calculation on a healthy breast, shown. This approach, using a time series segment as a model function, computes the percentage of variance for each individual pixel, representing the degree to which dynamic behavior is accounted for by the model function. Figure 8 shows the spatial distribution of the percentage of variance across the breast volume, using a single Valsalva mean oxyhemoglobin time series as the model function. Not unexpectedly, the Valsalva behavior is relatively uniform across the volume.

Derivative analysis was then done on the source-detector data for phases one, three and four separately for each Valsalva. The second phase was not analyzed in all cases as the presence of phase two depends on the length of Valsalva and was not present in all cases. The repeatability of the provocation was then examined by comparing separately the rank ordered plots for the derivative analysis of phases one, three and four. The close proximity of plot lines shows that over all three phases of the provocation the maneuver is repeatable. This is most interesting with respect to phase four, the slow return to baseline, being repeatable to a degree that the plot lines are overlying.

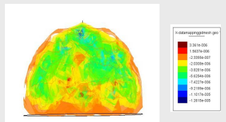

Figure 8. Percentage of variance using the oxyhemoglobin mean time series as a model function to identify Valsalva behavior across the image pixel space.

At this point, the first two of three requirements for a useful provocation, ability to effect the entire breast and repeatability, have been satisfied. The final requirement is that the provocation have the ability to differentiate healthy tissue from diseased. Continuing our examination of the dynamic behavior of phases one, three and four on a pixel level, three-dimensional data was analyzed for the same parameters as for the source-detector data. Based on a derivative analysis of the fourth phase of the valsalva on pixel data, the tumor bearing breasts of both subjects with cancer had more a gradual return to baseline than the healthy breast of the same patient. Derivative analysis of phase four using pixel data for the two healthy patients and the two patients with non-neoplastic breast disease did not yield a difference in one breast versus the other. Therefore the Valsalva has the ability to differentiate tumor bearing breast from healthy breast and non-neoplastic diseased breast.

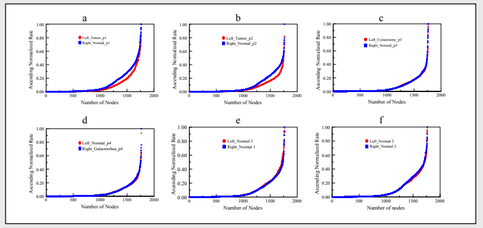

Figure 9. Comparison of rank-ordered normalized Phase 4 slopes for deoxygenated hemoglobin for study participants. (a,b = tumor bearing vs. normal breast tissue, c = post-cystectomy vs. normal breast tissue, d = galactorrhea vs. normal breast tissue, e,f = normal breast tissue).

Figure 9 illustrates this point by showing rank-ordered normalized Phase 4 slopes for the case of deoxygenated hemoglobin for six study subjects, with the subject's normal breast serving as a control. Panels 9(a) and 9(b) show the comparison of tumor-bearing versus healthy breast, clearly demonstrating the delayed return to baseline, present in neoplastic tissue, suggesting altered vascular reactivity. In contrast, the breast tissue of subjects with benign breast disease (9(c) and 9(d)) and those with healthy breast tissue (9(e) and 9(f)) have superimposable curves, without appreciable difference between left and right breasts.

The final step in our analysis of healthy and diseased breast tissue involved reconstruction of three-dimensional images using the data from the derivative analysis done on phase four of the Valsalva.

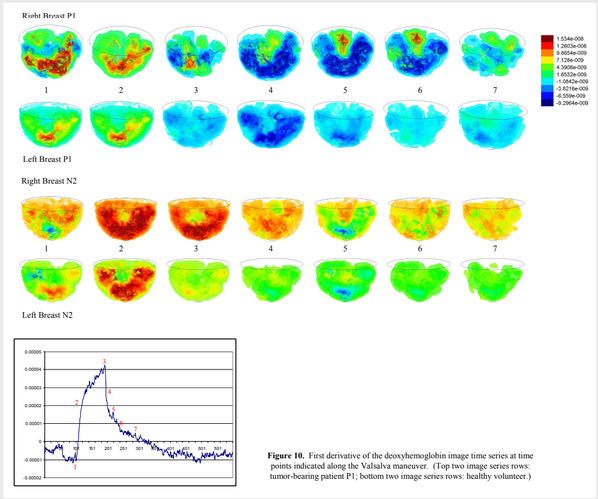

Figure 10. First derivative of the deoxyhemoglobin image time series at time points indicated along the Valsalva maneuver. (Top two image series rows: tumor-bearing patient P1; bottom two image series rows: healthy volunteer.)

Figure 10 illustrates a computation of the first time derivative of the deoxyhemoglobin time series at each pixel location, for the time points indicated along the Valsalva maneuver. The upper two image rows, calculated for the right tumor-bearing breast (top row), indicate a heterogeneous response which highlights the probable location of neoplastic tissue. This is most clearly evident in the right breast images 5 and 6 of the top row in figure 10. The second row of images, calculated for the normal (left) breast demonstrate greater homogeneity, expected of disease-free tissue. The difference in right and left dynamic behavior becomes more obvious in the Phase 4 region of the Valsalva. As such, we may expect that a discriminating metric might best be derived from this region of the Valsalva maneuver, satisfying the third and final criterion for derivation of a useful provocation for optical tomographic detection of breast cancer. For comparison, the third and fourth rows illustrate the homogeneous response of healthy breast tissue.

CONCLUSIONS

Near-infrared imaging with DYNOT technology can be used to analyze the dynamic changes induced in breast tissue by provocative maneuvers such as the Valsalva. This maneuver has been well-described in the literature and is characterized by four distinct phases, each of which corresponds to a physiologic process which may be independently modeled. The percentage of variance of the mean times series over the Valsalva using the mean time series as the model function shows that the provocation effects the entire breast. The effect from the Valsalva is repeatable as is shown by the rank ordered comparison of separate epochs for phase one, three and four. Examination of the image pixel data for phase four shows variation between tumor bearing breast and normal breast, with tumor bearing breast showing a more gradual return to baseline. The same analysis on healthy and on non-neoplastic disease breast show no variation in phase four between the breasts. Image reconstructed analysis of the transition from phase three to four yields a reconstructed three dimensional map that allows for localization of the tumor within the breast.

REFERENCES

1. R. L. Barbour, H. L. Graber, C. H. Schmitz, F. Tarantini, G. Khoury, D. J. Naar, T. F. Panetta, T. Lewis, Y. Pei, "Time–frequency analysis of functional optical mammographic images," in *Optical Tomography and Spectroscopy of Tissue V (Proceedings of SPIE, Vol. 4955)*, B. Chance, R. R. Alfano, B. J. Tromberg, M. Tamura, E. M. Sevick-Muraca, Eds., pp. 84–95 (2003).

2. Gindea AJ, Slater J, Kronzon I, " Doppler echocardiographic flow velocity measurements in the superior vena cava using the Valsalva maneuver in normal subjects ," *Am J Cardiology* 65(20), 1387-91 (1990).

3. H. L. Graber, Yaling Pei, Randall L.Barbour, David K.Johnston, Ying Zheng, John E,Mayhew "Signal source separation and localization in the analysis of dynamic near-infared optical tomographic time series," in *Optical Tomography and Spectroscopy of Tissue V (Proceedings of SPIE, Vol. 4955)*, B. Chance, R. R. Alfano, B. J. Tromberg, M. Tamura, E. M. Sevick-Muraca, Eds., pp. 31-51 (2003).

ACKNOWLEDGEMENTS

This work was supported by the National Institutes of Health (NIH) under Grants 5R21-HL67387-01, 1R21-DK63692 and R41-CA96102, by the US Army under Grant DAMD017-03-C-0018, and by the New York State Department of Health.